Chemosphere 272 (2021) 129794

Contents lists available at ScienceDirect

Chemosphere

journal homepage: www.elsevier.com/locate/chemosphere

Hg(II) sensing, catalytic, antioxidant, antimicrobial, and anticancer potential of *Garcinia mangostana* and α-mangostin mediated silver nanoparticles

Nargis Jamila [a, *], Naeem Khan [b, **], Nousheen Bibi [c], Muhammad Waqas [d], Sadiq Noor Khan [e], Amir Atlas [b], Farhat Amin [c], Faryal Khan [a], Malka Saba [a]

[a] Department of Chemistry, Shaheed Benazir Bhutto Women University, Peshawar, 25000, Khyber Pakhtunkhwa, Pakistan
[b] Department of Chemistry, Kohat University of Science and Technology, Kohat, 26000, Khyber Pakhtunkhwa, Pakistan
[c] Department of Bioinformatics, Shaheed Benazir Bhutto Women University, Peshawar, 25000, Khyber Pakhtunkhwa, Pakistan
[d] Department of Botanical and Environmental Science, Kohat University of Science and Technology, Kohat, 26000, Khyber Pakhtunkhwa, Pakistan
[e] Department of Medical Lab Technology, University of Haripur, Haripur, 22060, Khyber Pakhtunkhwa, Pakistan

HIGHLIGHTS

- Synthesis of *G. mangostana* and α-mangostin AgNPs.
- Hg(II) sensing by synthesized AgNPs in real tap water samples.
- Catalytic property of synthesized AgNPs.
- Significant anticancer activity against DU-145 cell line by subject AgNPs.
- Validation of anticancer activity via molecular docking analysis.

GRAPHICAL ABSTRACT

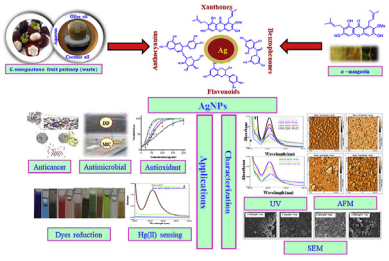

ARTICLE INFO

Article history:
Received 17 October 2020
Received in revised form
17 January 2021
Accepted 23 January 2021
Available online 28 January 2021

Handling Editor: Derek Muir

Keywords:
α-mangostin
AgNPs
Hg(II)
Dyes
Molecular docking

ABSTRACT

This study reports synthesis of *Garcinia mangostana* fruit pericarp (unwanted waste material) and α-mangostin mediated silver nanoparticles (AgNPs). These AgNPs were efficiently produced using 1:10 (extract and salt) ratio under stirring and heating, which was confirmed by surface plasmon resonance (SPR) band in UV–Visible spectroscopic analysis, and size of 73–91 nm determined by scanning electron microscopy (SEM) and atomic force microscopy (AFM). The synthesized AgNPs were used for Hg(II) detection in tap water, where the limits of detection and quantification were 2.6 μM and 8.9 μM, respectively. Furthermore, the subject AgNPs showed promising catalytic activity in the reduction of dyes and food colours including Congo red (CR), methylene blue (MB), malachite green (MG), methyl orange (MO), *para*-nitrophenol (PNP), rhodamine B (RdB), zarda yellow (ZY), deep green (DG), and bright red (BR). The synthesized AgNPs were also evaluated for their antioxidant, antimicrobial, and anticancer properties, where α-mangostin and its nanoparticles (Mang-AgNPs) exhibited promising IC_{50} values of 14.1 and 13.5 μg/mL, respectively against DU-145 cell line validated by in silico molecular docking study. This study is the first report highlighting the application of AgNPs of *G. mangostana* fruit pericarp extracts, and α-mangostin in Hg(II) detection, dyes degradation, and anticancer potential against DU-145.

* Corresponding author.
** Corresponding author.
E-mail addresses: njk985@gmail.com, nargisjamila@sbbwu.edu.pk (N. Jamila), nkhan812@gmail.com, naeem@kust.edu.pk (N. Khan).

https://doi.org/10.1016/j.chemosphere.2021.129794

Finding of this study suggested the suitability of AgNPs as promising solid biosensor in Hg(II) metal detection, dyes reduction, and target in anticancer drug development.

1. Introduction

Currently, metal nanoparticles (MNPs) have attracted considerable attention due to their unique physicochemical properties, which can be used in various science disciplines including electric devices, drug delivery, household, pharmaceuticals, and personal care products. Therefore, there is an increasing demand to develop ecofriendly methods for the synthesis of nanoparticles. Biosynthesis of MNPs using flora has been considered as a possible ecofriendly approach as compared to physicochemical methods (Ahmad et al., 2019; Vo et al., 2020). Due to the environment safety and production on large scale, biological methods using bacteria, fungi, algae, enzymes and plant extracts for the synthesis of nanoparticles is preferred over physical and chemical methods, which use poisonous chemical substances and non-polar solvents producing sludge in huge quantities with secondary contamination problems (Gahlawat and Choudhury, 2019). Thus, being the cheaper and eco-friendlier strategy, green chemistry and bio-approaches, which utilize plants and microbes for nanoparticles synthesis will reduce the usage of hazardous chemicals, and ultimately remediate the soils and ground water polluted with organic contaminants, dyes, and toxic metals (Ajaz et al., 2020). In addition, secondary metabolites such as polyphenols, terpenoids, and alkaloids present in various plant parts possess high stability and reducing ability, thus, act as potential candidate for the green synthesis of MNPs (Guo et al., 2014).

Among the MNPs, silver nanoparticles (AgNPs) have received a great attention because of wide range of applications in catalysis, degradation of environmental pollutants, sensing, drug delivery, cancer therapy, and antimicrobial properties (Abbasi et al., 2016; Venugopal et al., 2017; Priya et al., 2020). The recent advances in MNPs include their application in cancer therapy. In this regards, AgNPs as nano probes showed great potential towards sensing and imaging of tumors, vectors for the drug delivery, and suppressing tumor growth (Jahangirian et al., 2017). In addition, the antimicrobial activity of AgNPs allows them to be useful in numerous household products and in medical devices. Due to the similarity of their dimensions and shapes to several biological structures (membrane cell genes, proteins, and viruses), MNPs have been proposed to investigate biological processes, and sensing and treating diseases (Yoo et al., 2011).

The rapid advancement in technology, industrialization, and anthropogenic activities has resulted the release of significant amount of toxic metals such as arsenic (As), cadmium (Cd), mercury (Hg), and lead (Pb), thus, contaminating the living system, and have toxic effect on animals, plants and humans even at very low concentration (Sarwar et al., 2017). Among these toxic metals, Hg is a hazardous pollutant and bioaccumulative neurotoxin and ranked 3rd of the most toxic elements threatening the health of human population (Es'haghi et al., 2016). In addition to the toxic metals, dyes, which are conjugated compounds and industrial contaminants, also pose toxic effects towards human as well as aquatic ecosystems (Priyadarshini and Pradhan, 2017). Therefore, to ensure the environment safety, designing robust and efficient methods for its monitoring, quantifying, and removal are necessary. Commonly, $NaBH_4$ is used as a reducing agent but the reduction rate is kinetically unfavourable. On other side, MNPs, due to their increased surface area and well-dispersed size, have been widely used in colorimetric and chemical sensing of the toxic metal ions (Priyadarshini and Pradhan, 2017; Khan et al., 2019).

Garcinia mangostana (purple mangosteen, queen of fruits), belonging to Clusiaceae family has wide medicinal applications of curing abdominal disorders, infected wound, ulcer, hepatitis, and infections (Jamila et al., 2014; 2016; Tousian et al., 2017; Chen et al., 2018). It has been reported to be a rich source of xanthones, with the α-mangostin (Fig. 1a) as major compound, which perform significant antioxidant, antimicrobial, hepatoprotective, cardioprotective, anti-inflammatory, anti-Alzheimer's, anti-hyperglycemic, and cytotoxic properties (Tousian et al., 2017; Chen et al., 2018). Several research extensively explored the synthesis of AgNPs using *G. mangostana* extracts (Veerasamy et al., 2011; Rajakannu et al., 2015; Lee et al. 2016, 2019; Park et al., 2017). However, little information are available on the use of NPs for metal detection and dyes degradation (Sengan et al., 2018; Chandraker et al., 2019; Bandi et al., 2020). In addition, the *G. mangostana* fruit pericarp mediated AgNPs for Hg(II) detection and dyes degradation has never reported in the literature.

Considering the need of removal of toxic mercury and dyes from the environment, and pharmacological importance of *G. mangostana*, the present study was designed to synthesize *G. mangostana* fruit pericarp (unwanted waste material) aqueous extract AgNPs (GMAE-AgNPs), olive oil extract AgNPs (OOGM-AgNPs), and coconut oil extract AgNPs (COGM-AgNPs) under different conditions. Furthermore, a major compound, α-mangostin (Fig. 1a) isolated from ethyl acetate extract of *G. mangostana* was used for nanoparticles synthesis (Mang-AgNPs). The synthesized GM-AgNPs and Mang-AgNPs were characterized using UV–visible spectroscopy (UV–Vis), Fourier transform infrared spectroscopy (FT-IR), scanning electron microscopy (SEM), and atomic force microscopy (AFM) techniques. The subject AgNPs were assessed for chromogenic detection of Hg(II) in real tap water sample and as catalyst in the reduction of dyes [Congo red (CR), methylene blue (MB), malachite green (MG), methyl orange (MO), Rhodamine B (RdB), *para*-nitrophenol (PNP)] and food colours [zarda yellow (ZY), deep green (DG), bright red (BR)]. In addition, the subject GM-AgNPs, Mang-AgNPs, and α-mangostin were also tested for antioxidant, antimicrobial, and anticancer activity against prostate cancer cell; DU-145. The anticancer activity was also further validated by molecular docking analysis.

2. Materials and methods

2.1. Samples collection

The whole fruit (including pericarp, arils, and seeds) of *G. mangostana* was procured from the local markets of Malaysia and South Korea. The pericarp was separated from the arils, cleaned, properly labelled, and kept in refrigerator for further use.

2.2. Chemicals, reagents and instrumentation

Different types of solvents (*n*-hexane, dichloromethane, ethyl acetate, methanol and deionized water) were purchased from NAS Trading, Peshawar. Olive and coconut oils were procured from the

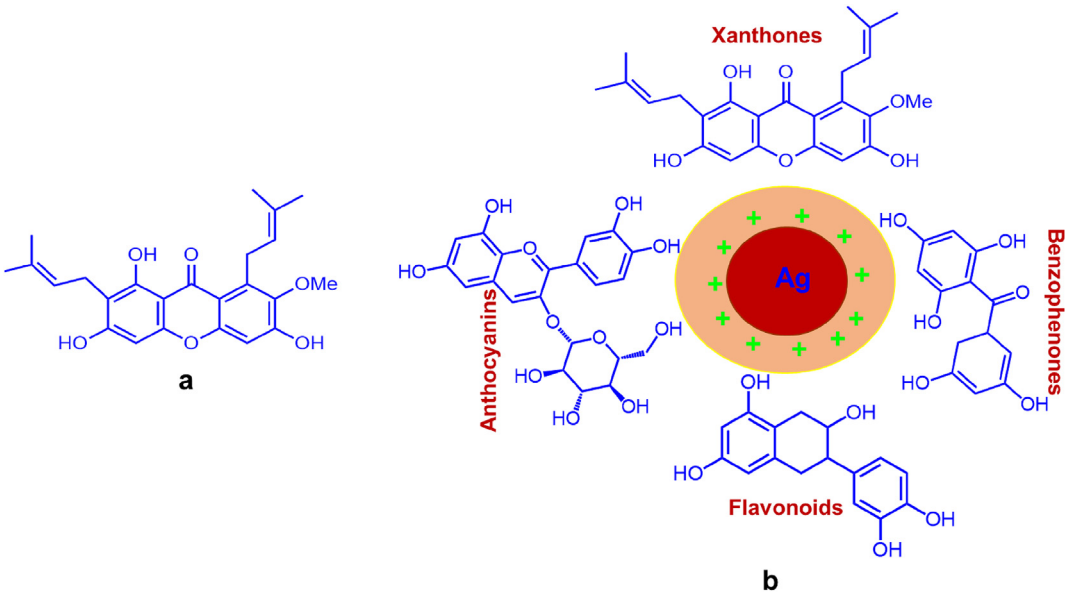

Fig. 1. (a) Chemical structure of α[fx]-mangostin, and (b) interaction between Ag^{+} and the active functional groups present in the *G. mangostana* peels extract (GM-AE) and the α-mangostin.

local market of Peshawar. Chemicals for AgNPs synthesis, antioxidant, antimicrobial, anticancer, and catalytic potential including $AgNO_3$, 2,2-diphenyl-1-picrylhydrazyl (DPPH), 2′-azino-bis-3-ethyl benzthiazoline-6-sulphonic acid (ABTS), gallic acid, trolox, DU-145 (prostate cancer cell line), L-929 (normal fibroblasts), $NaBH_4$, dyes; CR, MB, MG, MO, PNP, RdB, and standards (streptomycin, vancomycin, fluconazole, amphotericin) were purchased from Sigma-Aldrich (Steinheim, Germany) and Merck (Darmstadt, Germany). Food colours including BR, DG, and ZY were obtained from local market (Hypermall, Peshawar). Muller-Hinton agar (MHA) and broth (MHB) were purchased from Oxoid (England). The bacterial and fungal strains used for antimicrobial studies included *Bacillus subtilis* (Gram-positive), *Staphylococcus aureus* (Gram-positive), *Escherichia coli* (Gram-negative), *Pseudomonas aeruginosa* (Gram-negative), *Candida albicans*, *Candida krusei*, *Aspergillus flavus,* and *Trichophyton mentagrophyte* (Sigma Aldrich, USA). For AgNPs synthesis, antioxidant, and anticancer activities, a UV spectrophotometer (UV-1800, Shimadzu, Japan) was used. To confirm the involvement of the desired functional groups in AgNPs synthesis, the spectra were recorded in a range of 400–4000 cm^{-1} on FT-IR spectrometer (model Bruker). The size and surface topography of the synthesized AgNPs were analyzed by SEM (model JSM 5910), and AFM (Bruker Corporation) techniques. The processing and analysis of images was done by NanoScope™ software (version V614r1; Digital Instruments, Tonawanda, NY, USA).

2.3. Synthesis of GM-AgNPs and Mang-AgNPs

25 g of *G. mangostana* pericarp powder was separately macerated in 250 mL of deionized water, olive oil (as extracting solvent), and coconut oil (as extracting solvent). Each mixture was stirred at 500 rpm and 40 °C for 2 h to obtain aqueous, olive, and coconut oil extracts. These different extracts and a compound, α-mangostin were used to synthesize their corresponding AgNPs including GMAE-AgNPs, OOGM-AgNPs, COGM-AgNPs, and Mang-AgNPs. These AgNPs were synthesized through green synthesis approach under different conditions including mixing different ratios of the $AgNO_3$ salt solution and *G. mangostana* different extracts, stirring, heating and stirring, incubation (25–30 °C in dark), sunlight, different times (0 min–7 d) and pH (1–12). In the first trial, a mixture of 1:9 v/v (extract:salt) ratio was prepared and uniformly stirred at 60 °C for 30 min, 1 h–4 h, and so on. Similarly, a ratio of 1:10 v/v (extract:salt) resulted in NPs formation preliminary indicated by colour change from yellow to dark brown (Figure S1, supplementary material). In addition, the effect of pH (1–12) and time (0 min–72 h) on the subject AgNPs were investigated. The original pH of the synthesized AgNPs was in acidic range (3.5–5.0). The media pH (1–12) was varied with buffers. The synthesized AgNPs were collected from the whole solution by centrifugation and thorough washing with deionized water. The final product was dried in vacuum oven and stored in airtight vial for further analysis.

2.4. Hg(II) detection by GM-AgNPs and Mang-AgNPs, and analytical performance

The practical applications of the synthesized AgNPs were determined for Hg(II) ions recognition in the samples of routine tap water collected from village Ganderi Khattak, District Karak, Khyber Pakhtunhwa, Pakistan. The spiking of the samples was carried out with Hg(II) ions solution (0.1 mM). To analyze AgNPs sensing for Hg(II) ions detection, the different salt solutions (0.1 mM); Ag(I), Co(I), Cu(I), Na(I), K(I), Rb(I), Ba(II), Cd(II), Fe(II), Sb(II), Sb(III), Fe(III) were mixed with AgNPs in 1:1 (v/v) ratio. Sensitivity of the method for Hg(II) sensing was determined by analyzing Hg(II) solutions in a concentration range of 1.0 μM–50 μM. The limits of detection (LOD) and quantification (LOQ) were calculated as three and ten times standard deviations from ten replicates of blank per slope of the calibration curve.

2.5. GM-AgNPs and Mang-AgNPs as catalysts in dyes reduction

The catalytic activity of the synthesized AgNPs against the model pollutants including CR, MB, MG, MO, PNP, RdB dyes, and BR, DG, ZY food colours was analyzed according to the published literature (Khan et al., 2019). Briefly, 2.5 mL of 0.1 mM of the dyes and food colours were separately mixed with 0.5 mL of $NaBH_4$ (0.1 mM) in a UV–Vis cuvette. To this solution, 2 mg of the subject AgNPs were added to the cuvette and then checked their catalytic

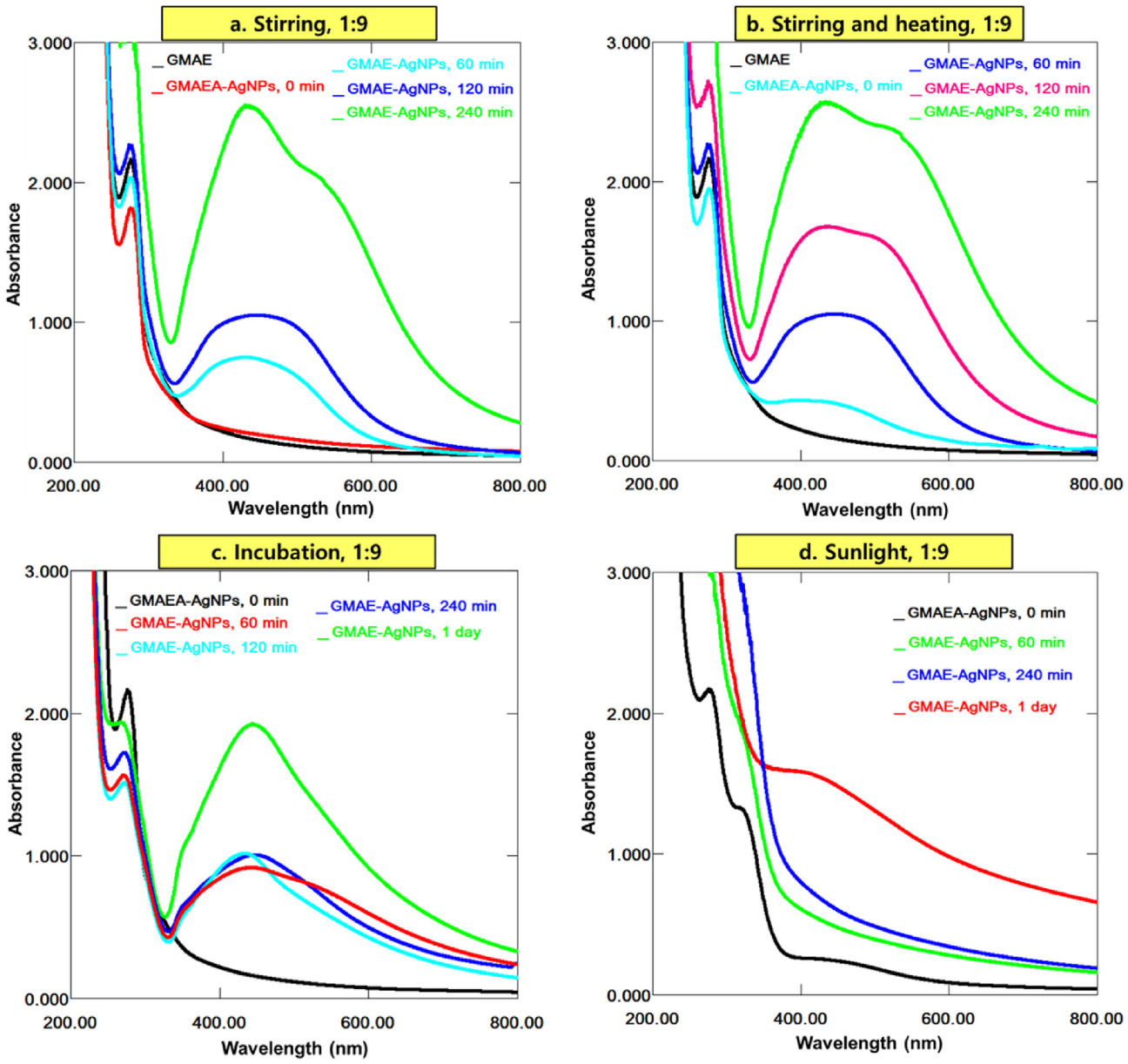

Fig. 2. UV spectra of GMAE-AgNPs (1:9 ratio) under (a) stirring, (b) heating + stirring, (c) incubation, (d) sunlight (e) stirring; GMAE-AgNPs (1:10 ratio) under (f) heating and stirring, (g) incubation, and (h) sunlight; (i) OOGM-AgNPs (1:10 ratio) under heating + stirring, (j) COGM-AgNPs (1:10 ratio) under heating + stirring, (k) pure α[fx]-mangostin in deionized water, ethyl acetate and ethanol, and (l) Mang-AgNPs (1:10 ratio) under heating + stirring.

potential. The reduction of dyes was indicated by discoloration and recorded by UV−visible spectrophotometer. The % decolourization/reducion of the dyes was calculated through the equation (1).

$$\%\text{decolourization/reduction} = (1 - A_t / A_0) \times 100 \quad (1)$$

where A_0 is the initial absorbance of dye and A_t is the absorbance of dye at time t.

2.6. Antioxidant and antimicrobial activities

For antioxidant and anticancer activities, the stock solutions of the AgNPs were prepared by dissolving 1 mg of the subject AgNPs in 1 mL of distilled water followed by sonication. Then, different concentrations in the range of 5–1000 ppm were prepared. For antioxidant activities evaluation, free radicals, DPPH and ABTS were used following the established procedure (Jamila et al., 2014). DPPH solution of 1.1 absorbance at 515 nm was prepared by dissolving approximately 20 mg in 250 mL methanol. A series of different concentrations (50–1000 μg/mL) of standards (gallic acid and trolox) and samples were also prepared. The reaction mixtures were prepared by mixing 150 μL of standard and samples with 2850 μL of DPPH radical solution and incubated in dark at ambient temperature for 24 h. A blank (methanol) and a control (DPPH solution) were also measured at intervals during analysis. The absorbance of the reaction mixtures in triplicate was measured at 515 nm and for inhibition percentage (%inhibition) calculation, the following equation (2) was used.

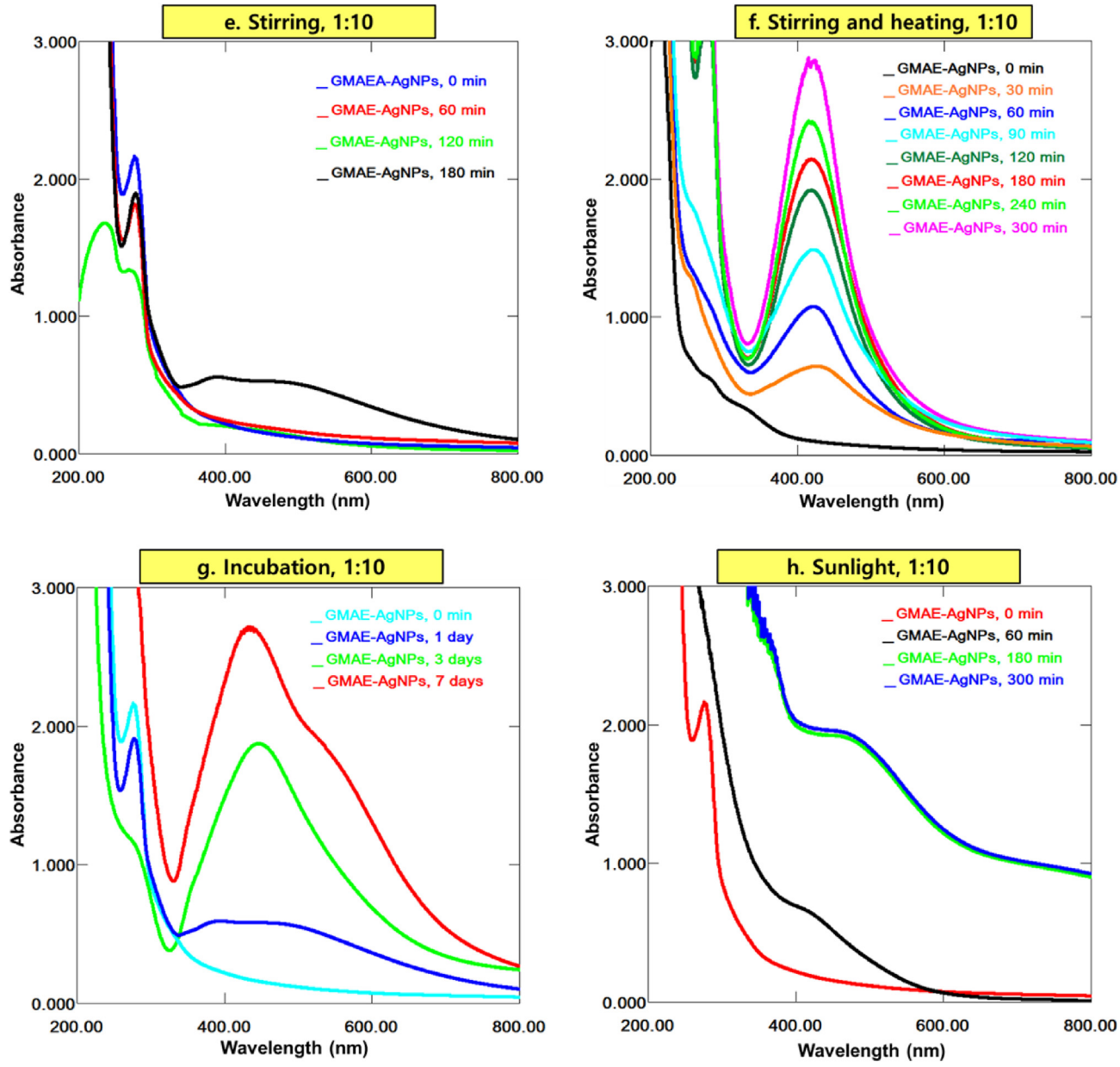

Fig. 2. (*continued*).

$$\%\text{inhibition} = \left(1 - A_{sample}/A_{control}\right) * 100 \quad (2)$$

The IC_{50} values were calculated using Graphpad Prism 7 by using %inhibition against the corresponding concentration and represented in μg/mL.

Antimicrobial activities were evaluated using disc diffusion (DD) and minimum inhibitory concentration (MIC) methods. Prior to the activities, the glassware was decontaminated using aqua regia (HCl/HNO_3) and deionized water. In DD, a 100 μL inoculum was streaked on MHA surface and loaded with sterile paper disc impregnated with 20 μL of test samples (2 mg/mL) and the standards in triplicate. The petri dishes were then incubated at 37 °C overnight. Inhibition zones were recorded in millimeters (mm). In MIC, a 96-well plate was used.

2.7. Anticancer activity and molecular docking validation

Anticancer activity of the synthesized AgNPs was analyzed using LDH assay (Jamila et al., 2014). The AgNPs solutions (1–50 μg/mL) were prepared in DMSO and tested against DU-145 and L-929 cell lines by measuring lactate dehydrogenase (LDH) released by damaged cells.

2.7.1. Molecular structures of receptor, ligand and AgNPs

The three-dimensional structure of lactate dehydrogenase (LDHA) was retrieved from protein data bank (PDB) (https://www.rcsb.org) with PDB ID:4jnk, while the structure of ligand was retrieved from PubChem database (https://pubchem.ncbi.nlm.nih.gov/). Energy minimization and structure refinements were made using GROMMACS available in Chimera 1.5.6 (Pettersen et al., 2004), and VEGA ZZ (http://www.ddl.unimi.it). Software for

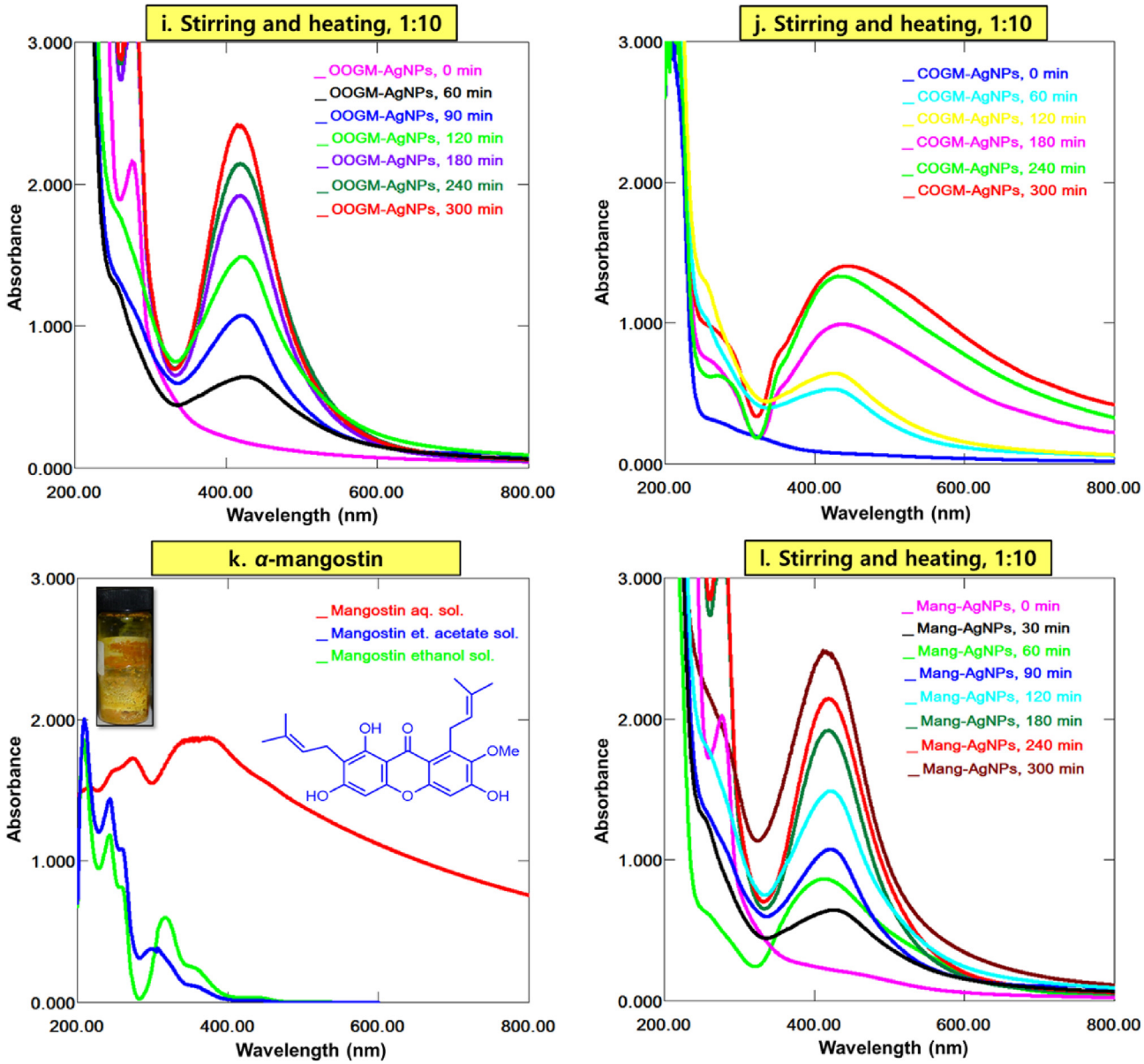

Fig. 2. (*continued*).

Chemistry and Material (SCM) (https://www.scm.com/) and SAMSON (https://www.samson-connect.net/) were used to build the 3D model of AgNPs with the diameter of 4 nm by using the atomic model of PVP-coated AgNPs as template (Alexander et al., 2015).

2.7.2. Molecular docking

Molecular docking of selected ligand molecule with LDHA in the presence and absence of AgNPs were carried out using AutoDock4.0 (Morris et al., 2009). Polar hydrogen atom and Kollmann charges were added. Annealing parameters for hydrogen bonding and van der Waals interactions were set to 4.0 A° and 2.5 A°. The number of runs for each docking experiment was set to 100 with the default remaining docking parameters. After docking, the best docked complexes were selected based on binding free energy value. Molecular interactions were monitored using Discovery Studio visualizer (http://accelrys.com/products/collaborative-science/biovia-discovery-studio) and UCSF chimera (Pettersen et al., 2004).

2.7.3. Molecular dynamic MD simulations

MD simulations were performed to calculate the stability and structural fluctuations of the best docked complex of LDHA in comparison to apo (unbound) state. Root mean square deviation (RMSD) and root mean square fluctuation (RMSF) were evaluated using GROMACS 4.5 package to assess the stability and fluctuations of protein C-alpha atoms. TIP4P water model in a periodic box was used for solvation all over simulation experiments in addition to neutralization by Na^+ and Cl^- counter ions. To investigate the stability behaviour of apo and bound LDHA systems, VMD, PyMol (http://www.pymol.org), and GROMACS tools were used.

2.8. Statistical analysis

The obtained results of antioxidant and antimicrobial activities are reported as means ± standard deviations ($n = 3$). The mean significant differences (represented by superscript letters) between the obtained values were analyzed using ANOVA along with

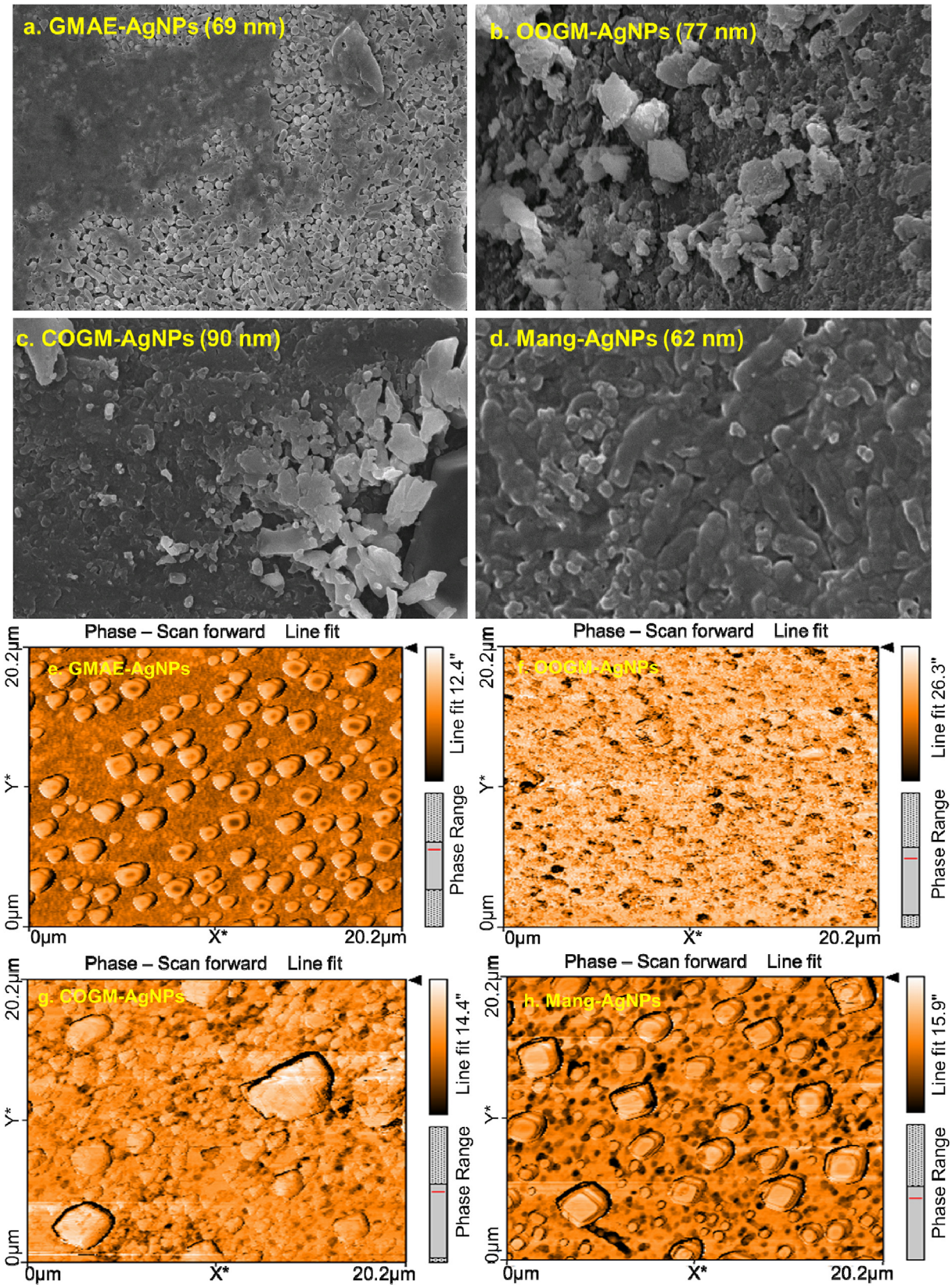

Fig. 3. SEM (a–d), and AFM images (e–h), and particle size distribution graphs (i–l) of the synthesized GM-AgNPs, OOGM-AgNPs, COGM-AgNPs, and Mang-AgNPs under heating and stirring.

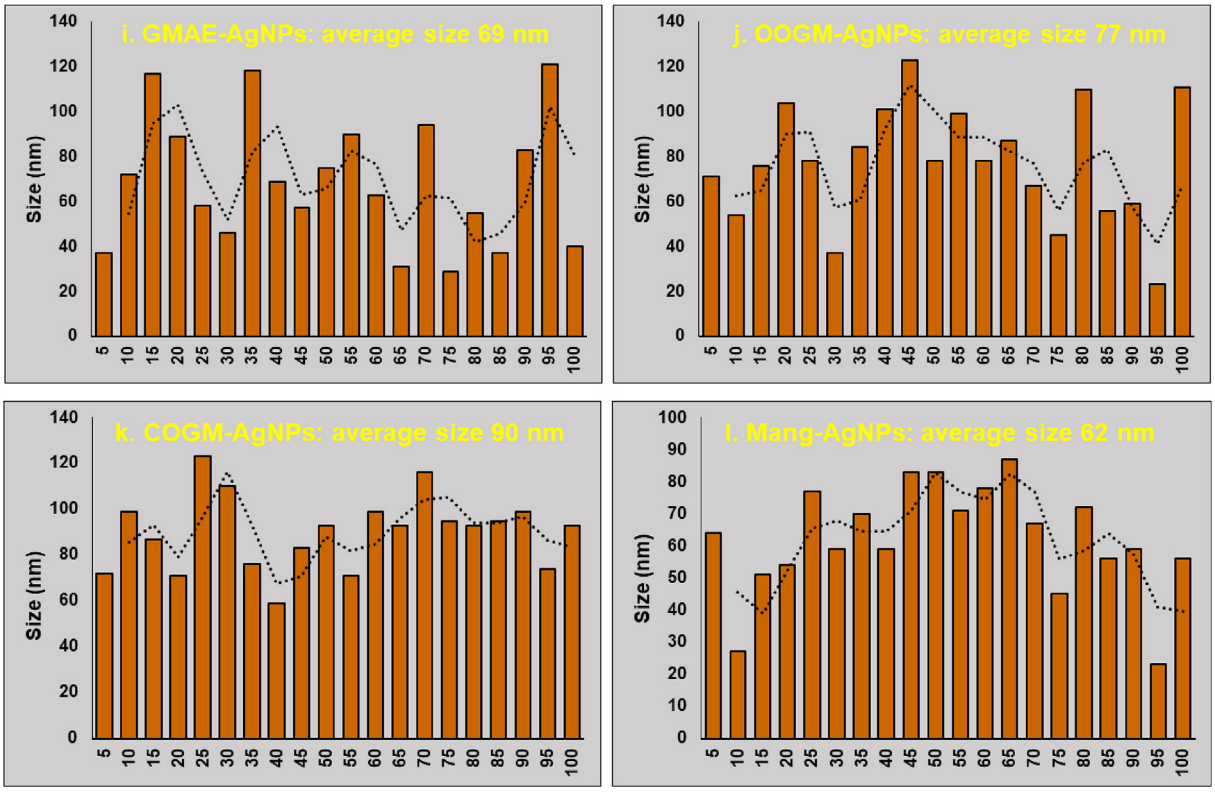

Fig. 3. (*continued*).

Tukey's HSD and Duncan's multiple range tests in SPSS, version 20.0 (SPSS Inc., Chicago, USA). The IC_{50} values were calculated with the help of GraphPad Prism 7 (GraphPad Software Inc., La Jolla, USA). Data are expressed with a significance level of $p < 0.05$.

3. Results and discussion

3.1. Synthesis and spectral properties of GM-AgNPs and Mang-AgNPs

G. mangostana is a rich source of polyphenolic compounds; xanthones, anthocyanins and flavonoids (Zarena and Sankar, 2012; Cheok et al., 2013). The hydroxyl group present in polyphenols could be available to reduce Ag^{+} through its oxidation in a way represented below (Lee et al., 2019).

$$Ag^{+} + R - OH \rightarrow Ag^{0} + R = O + H^{+}$$

Several studies have described the proposed mechanism for interaction of phenolic compounds with metal ions on NPs formation. For example, the hydroxyl group interaction, enol formation and liberation of reactive hydrogen, and oxidation of hydroxyl to carbonyl groups by adsorbing on the metal surface, NPs budding, aggregation, and bio-reduction have been reported to be responsible for $M^{+/++}$ reduction to M^{0}, and ultimately to NPs formation (Raghavan et al., 2015; Kumar et al., 2017). In addition, the efficiency of NPs formation and their biological activities, depend on the number and location/position of hydroxyl and carbonyl groups in the structure of phenolic compounds/xanthones (Jamila et al., 2014). The interaction between Ag^{+} and the active functional groups of several phenolic constituents including xanthones, flavonoids, benzophenones, and anthocyanins present in the *G. mangostana* pericarp extract proposed by Lee et al. (2019) is shown in Fig. 1b.

The synthesized AgNPs have shown that the ratios 1:9 and 1:10 under heating and stirring have significant role in AgNPs formation, preliminary indicated by colourimetric change from bright yellow to dull yellow to dark brown (Fig. 2). Furthermore, in both 1:9 and 1:10 ratios, stirring also resulted in AgNPs formation in slow rate. However, proceeding under sunlight, no GM-AgNPs were formed. The GM-AgNPs synthesized under stirring as well as heating and stirring, exhibited a prominent absorption peak at 433 nm, indicating the existence of AgNPs. The UV–Vis spectra of the mixtures were monitored at 1 h–5 h to 7 days. In UV analysis, the peaks get more intense with the passage of time, which is indicating high content of AgNPs. In 1:9 ratio, red/bathochromic shift from 430 nm to 580 nm was observed (Fig. 2a–d). This red shifted and broadened SPR band was a result of salt-induced AgNPs aggregation, also indicated by the colourimetric change of dull yellow to dark brown colour (Wang et al., 2010). Furthermore, this aggregation ultimately caused the depletion of stable GM-AgNPs due to increased interactions between GM extract having large amount of reductive phytoconstituents, and available silver ions (Lee et al., 2019). This led to a rapid AgNPs formation and subsequent growth through Ostwald ripening (Ramos-Sanchez et al., 2020; Rani et al., 2020). Proceeding the AgNPs synthesis with 1:10 ratio (Fig. 2e–h) of extract and silver salt solution, respectively, under heating and stirring, a sharp band at 433 nm was observed (Fig. 2f) to commensurate with surface plasmon excitations, ultimately the indication of stable AgNPs formation (Rani et al., 2020). The results depict that, 1:10 ratio of the extract and salt under heating and stirring appeared to be the best condition for the synthesis of GM-AgNPs as this mixture exhibited an intense sharp peak at 433 nm. The increased temperature (60 °C) suggests the rapid consumption of reactants to form the nuclei and generate small AgNPs rather than aggregates. Furthermore, the reaction temperature is the important factor affecting the AgNPs size as due to the homogenous

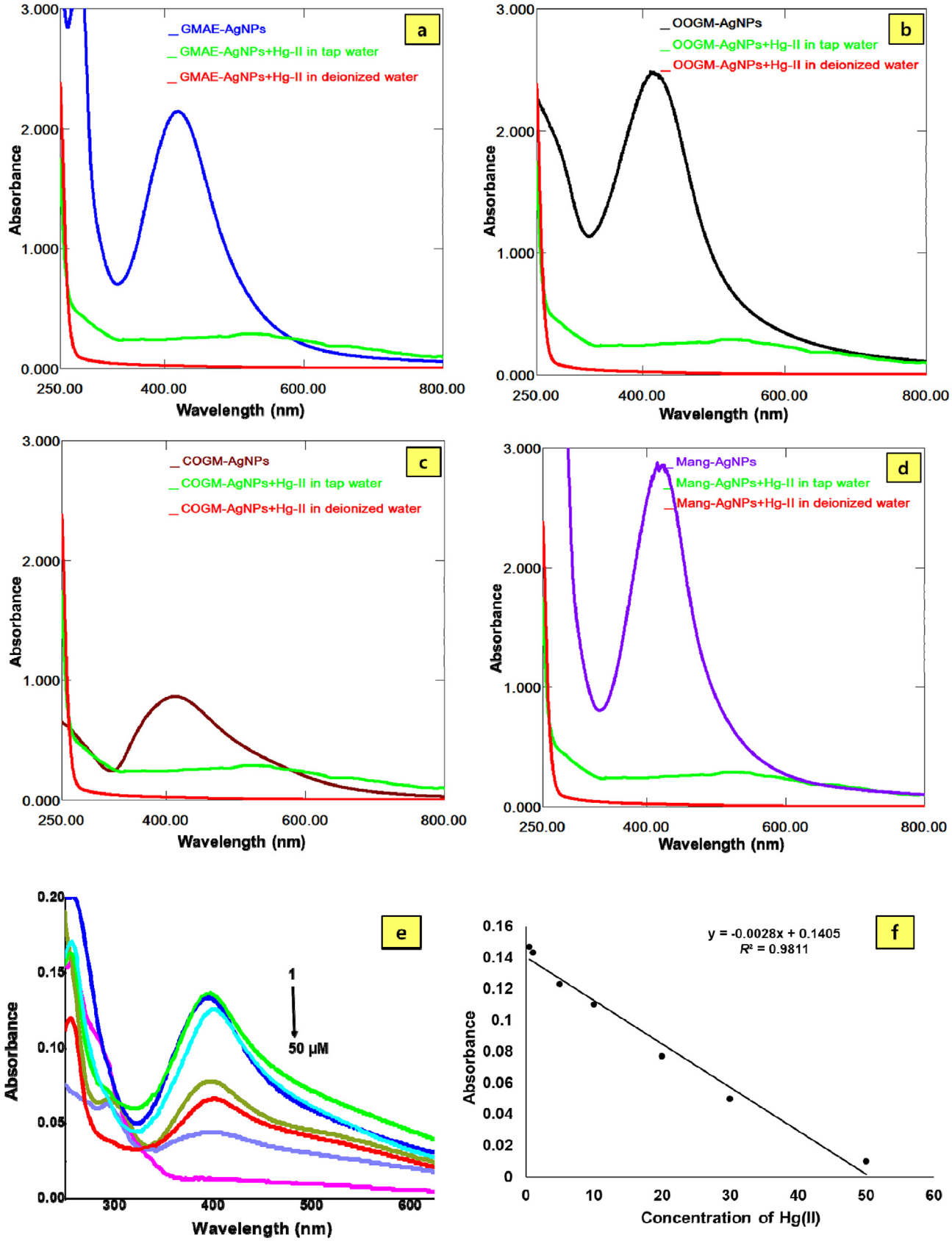

Fig. 4. UV–vis spectra of (a) GMAE-AgNPs, (b) OOGM-AgNPs, (c) COGM-AgNPs, (d) Mang-AgNPs detection system of Hg(II) in tap water samples, (e) UV–vis spectra of various concentration of Hg(II), and (e) regression plot of GM-AgNPs in response to various concentration of Hg(II).

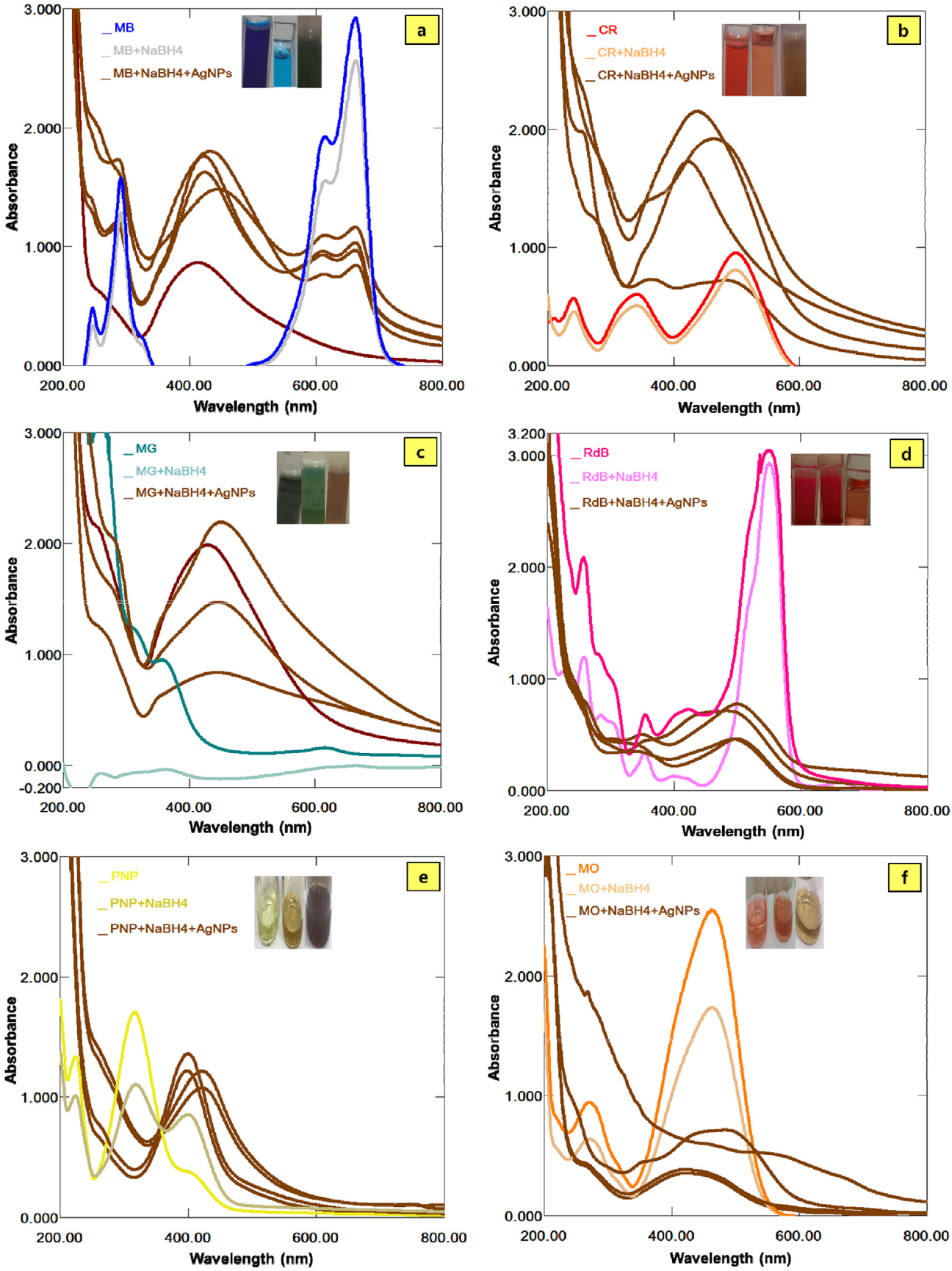

Fig. 5. UV–Vis spectra of the catalytic potential of GMAE-AgNPs, OOGM-AgNPs, COGM-AgNPs against dyes (a–f) and food colours (g–i). (For interpretation of the references to colour in this figure legend, the reader is referred to the Web version of this article.)

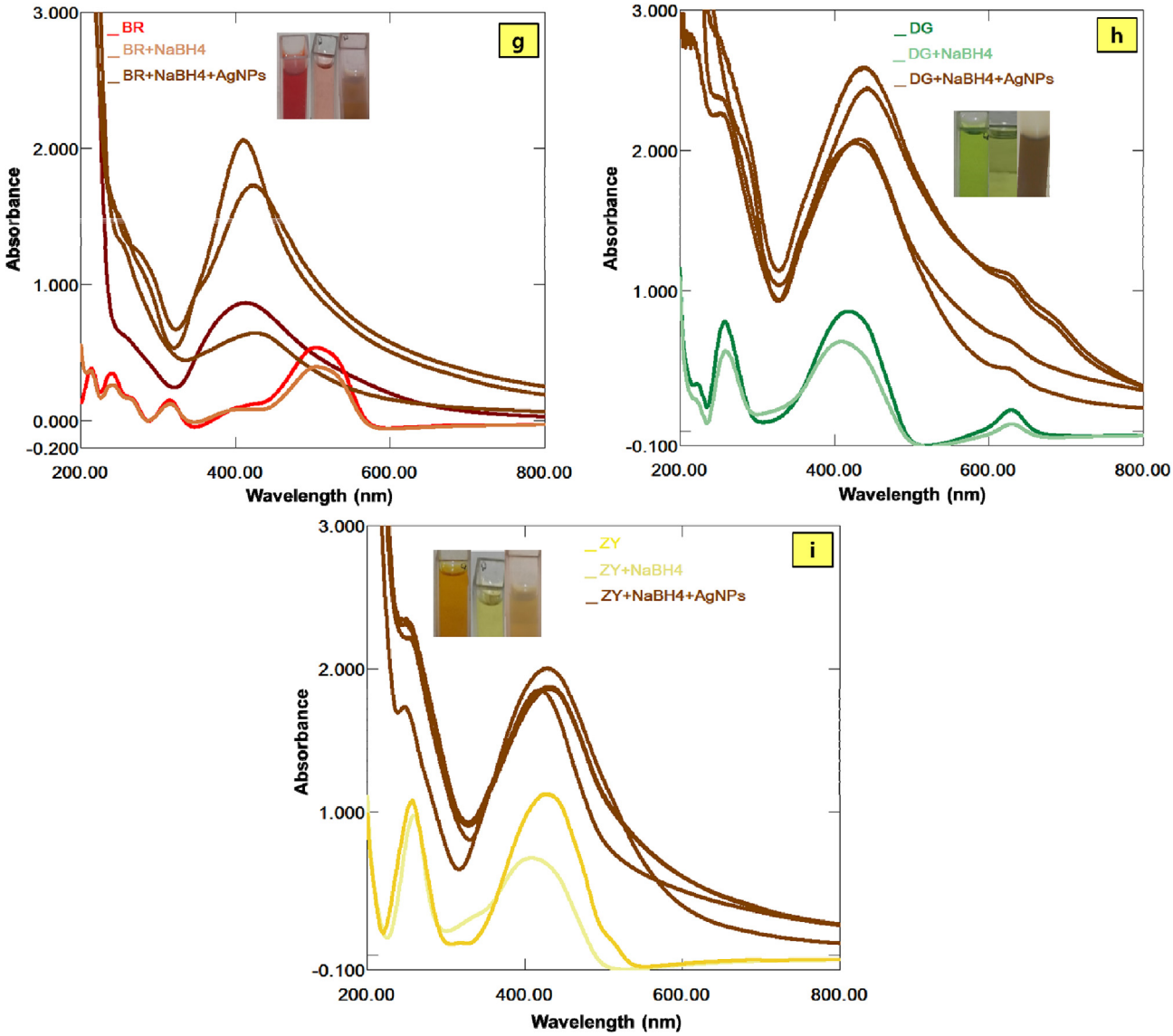

Fig. 5. (*continued*).

nucleation and rapid reduction of $AgNO_3$ at high temperature, lead to smaller AgNPs.

In this research work, the GM-AgNPs were also synthesized using olive and coconut oil as stabilizing agents as well as extracting solvents instead of deionized water. Oils contain different fatty acids, which can control the precipitation and agglomeration of AgNPs morphology. Olive and coconut oils are safer, easily available, and inexpensive. Previous literature reported that the olive oil-mediated AgNPs were stable for several months and in favor of homogeneous particles (Es'haghi et al., 2016). AgNPs utilizing olive and coconut oil (OOGM-AgNPs and COGM-AgNPs) were synthesized under the same condition of 1:10 ratio (extract and salt solution) as described previously. Among the conditions applied, under stirring and heating, prominent sharp peaks in case of olive as well as coconut oil exhibited at 430–450 nm in UV spectrometric analysis (Fig. 2i and j).

α-mangostin isolated from ethyl acetate extract of *G. mangostana* fruit pericarp and characterized by 1D and 2D NMR (Figures S2-S6, supplementary material) was also utilized for AgNPs synthesis. Significant AgNPs in a ratio of 1:10 were formed, primarily indicated by colour change (yellow [fx]→ dark brown). This reaction mixture exhibited an absorption peak at 430–450 nm in UV spectroscopic analysis (Fig. 2k and l), which could be typically SPR peak (Linic et al., 2015), indicating the significant reducing ability of α-mangostin. The combined vibrations of the mobile electron exist in the conduction band of metal oxide energetic by the incident UV radiation is responsible for surface plasmon absorption (Linic et al., 2015).

pH is the parameter, which greatly affects the surface morphology, aggregation, and capping and stabilizing potential of the NPs by varying the charge of chemical constituents present in the aqueous extract. A pH variation from 1 to 12 affected the absorption peak intensity and wavelength as shown in Figure S7 (supplementary material). However, for GM-AgNPs, a sharp intense absorption peak was obtained under basic conditions (pH 8 to 12).

3.2. Characterization of GM-AgNPs and Mang-AgNPs

In this study, FT-IR spectroscopy determined the functional groups, which participates in the reduction of $AgNO_3$ to AgNPs. The spectrum of GM-AE (Figure S8, supplementary material) exhibited

major stretching vibrations at 3500-3200 cm^{-1}, 2900-2800 cm^{-1}, and 1750-1600 cm^{-1} of the O–H, C–H and C=O groups of phytochemicals present in GM-AE. The O–H absorption frequencies are due to the presence of phenolic compounds including xanthones, anthocyanins, and flavonoids in GM-AE. When the spectra of the extract and the AgNPs (Figure S8) were compared, it was found that absorption bands exhibited at 3500-3200 cm^{-1} and 1750-1600 cm^{-1} have changed in shapes and somehow disappeared. The absorption bands in the region of 1600 cm^{-1} to 1400 cm^{-1} confirmed the aromatic structures present in GM-AE. Additionally, as shown in Figure S8 (supplementary material), FTIR spectra of α-mangostin and its AgNPs are almost similar but with the difference of reduction in intensities of specified absorptions. FT-IR spectrum of α[fx]-mangostin exhibited a number of prominent peaks in the range of 3500–3200 cm^{-1}, 2900-2800 cm^{-1}, and 1750-1600 cm^{-1}, which is due to O–H, C–H, and C=O stretch (Samprasit et al., 2018). Comparing the spectra of Mang-AgNPs with that of α-mangostin, there is a reduction and shape changes in the absorption bands exhibited at 3500-3200 cm^{-1} and 1750-1600 cm^{-1} for O–H, and C–O stretching. This indicates the involvement and interaction of these groups in the formation of AgNPs. The SEM and AFM analyses for the size and morphological determination of GMAE-AgNPs, OOGM-AgNPs, COGM-AgNPs, and Mang-AgNPs showed that these nanoparticles are spherical, which display sizes of 69, 77, 90, and 62 nm (Fig. 3), respectively. Fig. 3 further shows two-dimensional AFM images of the subject AgNPs, which indicates that the surface morphologies of the GM-AgNPs are roughly spherical with no any significant difference. The average sizes of the synthesized AgNPs were 62–90 nm with Mang-AgNPs as the smallest (62 nm) among the subject GM-AgNPs.

3.3. Detection of Hg(II) ions via GM-AgNPs and Mang-AgNPs in tap water samples

The sensing of Hg(II) ions via GM-AgNPs and Mang-AgNPs, showed that upon the addition of Hg(II) to AgNPs, decolourization and the disappearance of SPR bands occurs. These colour and spectral changes could be due to induced destabilization and aggregation of GM-AgNPs with Hg(II), which is ultimately attributed to the electrochemical differences of Hg(II) (high reduction potential) and Ag^0 (low reduction potential). Hence, Hg(II) acts as oxidizing agent and could be detected via colorimetric sensing by UV–visible spectrophotometer (Bothra et al., 2014; Chandraker et al., 2019; Ismail et al., 2019). Sensing other metals, the Ag(I), Co(I), Cu(I), Na(I), K(I), Rb(I), Ba(II), Cd(II), Fe(II), Sb(II), Sb(III), Fe(III) cations did not cause any substantial colour and spectral changes, which could be attributed to the low reduction potential to act as oxidizing agents.

In real water samples, the results of Hg(II) ions sensing (Fig. 4a–d) of the spiked samples have shown a significant decrease in the SPR bands of GM-AgNPs within 10–15 min. In determining sensitivity of the method, a concentration range (1–50 μM) of Hg(II) showed a decrease as well as blue shifts in SPR absorbance (Fig. 4e). A linear graph constructed by plotting absorbance against concentration of Hg(II) (Fig. 4f) was $y = -0.0028x+0.1405$ with regression constant (R^2) of 0.9811. The LOD and LOQ in this method were 2.6 μM and 8.9 μM, respectively. Hence, the parameters represent its practical utility in Hg(II) sensing in water and other environmental samples.

3.4. Catalytic dyes reduction via GM-AgNPs and Mang-AgNPs

Synthetic dyes such as CR, MB, MG, MO, PNP, RdB released from textile, paper, cosmetics, and plastic industries are conventionally reduced through $NaBH_4$ to non-toxic species. However, this reduction proceeds with slow rate (Chandraker et al., 2019). On the other hand, recently, MNPs showed well-known and kinetically favourable catalytic activity in dyes reduction and removal by lowering the activation energy. For the AgNPs to be effective catalyst, its redox potential needs to be found between the redox potential of donor ($NaBH_4$) and the acceptor (dye) system (Bonnia et al., 2016). $NaBH_4$ as reducing agent supply electrons and reduction potential of dye molecules increases due to their adsorption on NPs, which supports the electron transfer from $NaBH_4$ to dyes. This causes decolourization of dye molecules by an oxidation–reduction reaction (Pandey et al., 2020). In this study, the degradation's rate of CR, MB, MG, MO, PNP, RdB, BR, DG, ZY dyes in the presence of $NaBH_4$ was observed in the presence and absence of GM-AgNPs and Mang-AgNPs as catalyst. The results (Fig. 5a–i) showed that dyes to which $NaBH_4$ was added in absence of GM-AgNPs and Mang-AgNPs occurred at an extremely slow rate and no any difference in colour with naked eyes was observed. Furthermore, UV–Vis analysis of this mixture after 30 min caused a very small decrease in the absorption maxima of dyes. However, on the addition of AgNPs, the significant absorption maxima decreased and the discoloration of dyes greatly enhanced within 5 min. The % reduction of the dyes calculated using equation (2) shows reduction of CR (86–92%), MB (79–85%), MG (89–95%), MO (89–96%), PNP (85–91%), RdB (88–93%), BR (80–87%), DG (79–86%), ZY (88–92%) by the synthesized AgNPs with the highest reduction percentage by Mang-AgNPs. This indicates that due to high volume to surface ratio, the synthesized AgNPs provide more catalytic sites and lower activation energy in dyes reduction. The discoloration of dyes was due to their reduction. For example, the disappearance of blue colour of methylene blue in solution is due to the reduction of methylene blue to colourless leucomethylene blue as shown in Figure S9.

3.5. Antioxidant and antimicrobial activities

The detailed antioxidant activity values of the GM-AE and GM-AgNPs assessed using DPPH and ABTS free radicals are given in Figure S10. From the results, it is seen that among the AgNPs, OOGM-AgNPs have shown strong inhibitions against DPPH free radical with IC_{50} value of 53.0 μg/mL, followed by GMAE-AgNPs and COGM-AgNPs (56.3 and 60.5 μg/mL). In this investigation, the GM-AE and its AgNPs were found the most active DPPH inhibitors. The antioxidant activity of α-mangostin and its AgNPs evaluated by DPPH free radical assay shows that Mang-AgNPs is the most active antioxidant agent against DPPH with IC_{50} value of 36.5 μg/mL, as compared to standards; gallic acid (IC_{50} = 41.7 μg/mL) and trolox (IC_{50} = 72.2 μg/mL). Determining the ABTS radical scavenging by AgNPs, it was found that as compared to DPPH radical, ABTS radical was significantly reduced by the subject AgNPs with the highest inhibition by Mang-AgNPs (IC_{50} = 27.9 μg/mL) followed by α-mangostin (IC_{50} = 30.8 μg/mL) and were statistically significant. Literature shows that the ABTS radical scavenging ability greatly depends on the number of hydroxyl groups, irrespective of their location/position in the structure of phenolic compounds (Jamila et al., 2014).

In antimicrobial activity, the inhibition zones of GM-AE, GMAE-AgNPs, OOGM-AgNPs, and Mang-AgNPs (10–23 mm) and MIC values (31.25–250.0 μg/mL) against bacterial strains confirmed that these NPs have high antibacterial activity. The GM-AE and their AgNPs were the most effective against Gram-positive strains as compared to Gram-negative with the least inhibitory effect against *P. aeruginosa* and *E. coli* as indicated by their zone of inhibition and MIC values (Table 1). In antifungal activity, α-mangostin, GM-AE, and their AgNPs were found active inhibitors against the tested fungal strains (Table 1). The most effective and significant

Table 1
Antimicrobial activity by disc diffusion (DD) and minimum inhibitory concentration (MIC) methods of GM-AE, GMAE-AgNPs, OOGM-AgNPs, COGM-NPs, α-mangostin, and Mang-AgNPs.

Samples	Disk diffusion (mm)				Minimum inhibitory concentration method (μg/mL)			
	S. aureus	B. subtilis	*P. aeruginosa*	*E. coli*	*S. aureus*	B. subtilis	*P. aeruginosa*	*E. coli*
GM-AE	12.0^{a}	12.0^{a}	7.0^{b}	7.0^{b}	125^{c}	125^{c}	500^{e}	500^{d}
GMAE-AgNPs	17.0^{c}	18.0^{c}	10.0^{c}	11.0^{d}	62.5^{b}	62.5^{b}	500^{d}	500^{c}
OOGM-NPs	18.0^{d}	18.0^{c}	10.0^{c}	11.0^{d}	62.5^{b}	62.5^{b}	500^{d}	500^{c}
COGM-AgNPs	14.0^{b}	12.0^{b}	6.0^{a}	6.0^{a}	125^{c}	125^{c}	1000^{e}	1000^{d}
α-mangostin	19.0^{e}	20.0^{d}	15.0^{f}	13.0^{e}	31.25^{a}	31.25^{a}	125^{b}	125^{b}
Mang-AgNPs	23.0^{g}	21.0^{e}	18.0^{g}	19.0^{f}	31.25^{a}	31.25^{a}	62.5^{a}	31.25^{a}
Vancomycin*	19.0^{e}	20.0^{d}	12.0^{d}	10.0^{c}	31.25^{a}	31.25^{a}	250.0^{c}	500^{c}
Streptomycin*	20.0^{f}	22.0^{f}	14.0^{e}	19.0^{f}	31.25^{a}	31.25^{a}	250.0^{c}	31.25^{a}
Antifungal activity								
Samples	Disk diffusion (mm)				Minimum inhibitory concentration method (μg/mL)			
	C. albicans	*C. krusei*	*A. flavus*	*T. mentagrophytes*	*C. albicans*	*C. krusei*	*A. flavus*	*T. mentagrophyte*
GM-AE	10.0^{c}	10.0^{c}	9.0^{c}	9.0^{b}	250^{b}	250^{b}	500^{c}	500^{c}
GMAE-AgNPs	9.0^{b}	9.0^{b}	8.0^{b}	9.0^{b}	500^{d}	500^{c}	500^{c}	500^{c}
OOGM-AgNPs	9.0^{b}	10.0^{c}	9.0^{d}	7.0^{a}	500^{d}	250^{b}	500^{c}	1000^{d}
COGM-NPs	8.0^{a}	7.0^{a}	7.0^{a}	9.0^{b}	500^{d}	1000^{d}	1000^{d}	500^{c}
α-mangostin	11.0^{c}	11.0^{d}	11.0^{e}	11.0^{c}	250^{b}	250^{b}	250^{b}	250^{b}
Mang-AgNPs	10.0^{c}	9.0^{b}	10.0^{d}	12.0^{d}	250^{c}	250^{b}	250^{b}	125^{c}
Fluconazole*	19.0^{d}	21.0^{f}	25.0^{f}	25.0^{f}	31.25^{a}	31.25^{a}	31.25^{a}	31.25^{a}
Amphotericin*	19.0^{d}	19.0^{e}	25.0^{f}	24.0^{e}	31.25^{a}	31.25^{a}	31.25^{a}	31.25^{a}

*represents standard drugs.
The superscript letters in a column represent significantly different values ($p < 0.05$) by Tukey's and Duncan's multiple range tests.

inhibition by the subject AgNPs against different microbes could be due to their increased surface area to volume ratio, which enhances its exposure to receptor sites (Pelgrift and Friedman, 2013). Furthermore, the mechanism of bacterial inhibition by AgNPs may be due to the soft acidic nature of Ag, which acts on the S and P bases of DNA, ultimately inactivates its replication, which leads to disability of the nuclear machinery of the cell (Sana and Dogiparthi, 2018).

3.6. Anticancer activity, molecular docking, and dynamics simulation analyses

The anticancer activity of the GM-AgNPs, α-mangostin, and Mang-AgNPs against DU-145 was evaluated for the first time. Table S1 and Figure S11, depict the significant toxicity of AgNPs towards DU-145 cells. A pure α-mangostin and its AgNPs tempted 100% cell death after the interval of 72 h treatment exhibiting IC_{50} values of 14.1 and 13.5 μg/mL, respectively. Furthermore, OOGM-AgNPs also caused 100% inhibition/cell death after 72 h. However, GM-AE, GMAE-AgNPs and COGM-AgNPs showed cytotoxic effect lower than 100% cell death (IC_{50} = 22.4 μg/mL). Compared to DU-145 cell, normal (L-929) cell death was 1–2%, which represents a selective action of the GM-AgNPs and Mang-AgNPs on DU-145 cancer cells. It is noteworthy that LDH, which is a cytoplasmic enzyme, plays a key role in pyruvate conversion to lactate. In case of any damage to cell membrane, this enzyme is released from the necrotic cell membranes and so, can be associated with cancers. Necrosis is an accidental cell death in which the intracellular content is released into extracellular milieu. Therefore, LDH activity is useful in gaining information on the dead and necrotic cells, and ultimately in anticancer activity (Lucky et al., 2015).

3.6.1. Molecular docking interaction analysis

To support the assumed mode of action for the subject α-mangostin and its AgNPs, to predict the effective antitumour hit, and to get deep understanding of the inhibitory mechanism of α-mangostin with LDHA active site, molecular docking was performed. All the docked conformations were clustered pretty well within the same binding site of the native co-crystallized ligand (Fig. 6a). Binding affinity was determined through hydrogen bonding and RMSD score. Binding analysis of the best docked conformation of α−mangostin in complex with LDHA revealed strong binding affinity with good binding free energy score of −9.87 kcal/mol. Ala95 and Gly96 of LDHA protein formed two H-bond (2.7 Å and 2.5 Å respectively) with the 1-hydroxy moiety of α-mangostin. His192 ns Asn197 formed coordinate covalent bond with the 6-hydroxyl group of α-mangostin in addition to one H-bond (2.0 Å) formed by Asn197 with the oxygen group. All the H-bond distances measured were between 1.5 and 3.0 Å indicating strong binding. Apart from these number of residues, for example, Gly28, Ala29, Val30, Arg98, Leu164, Ile251, Thr247 formed hydrophobic interactions with α-mangostin to keep it within the binding pocket of protein (Fig. 6b and c). Drug coated with AgNPs was used for sustainable release and improved therapeutic potential. The results of molecular docking for binding affinity of LDHA with Mang-AgNPs showed strong affinity of Mang-AgNPs towards the catalytic cavity of LDHA with binding free energy of −10.67 kcal/mol. The number of non-bonded contacts between the α-mangostin and Mang-AgNPs were observed within 5 Å as shown in Fig. 6d and e with no impact on the structure of α-mangostin. Comparison of binding region and binding residues of LDHA with α-mangostin and its AgNPs showed that most of the binding residues were unaltered, inferring that the presence and absence of AgNPs does not affect the binding affinity and binding orientation of LDHA with α-mangostin (Fig. 6f). Overall, the docking of α-mangostin could trigger conformational alteration of LDHA active sites, leading to a reduction of their catalytic activity, and these findings correlate to their experimental anticancer activity results, indicating the potential of α-mangostin being use as drug for cancer therapeutics.

3.6.2. Molecular dynamics simulation analysis

To investigate the stability and structural fluctuations of the bound and unbound state of LDHA systems, molecular dynamics simulation was performed. Root mean square fluctuation (RMSF) and root mean square deviations (RMSD) of c-alpha atoms of LHDA trajectories were measured to estimate the stability and fluctuations of the both systems (bound and unbound). Using unbound state as reference, RMSF and RMSD of bound LDHA system was calculated at 10 ns. Detailed analysis of dynamic trajectory of unbound and bound LDHA showed over all stability in the RMSF with

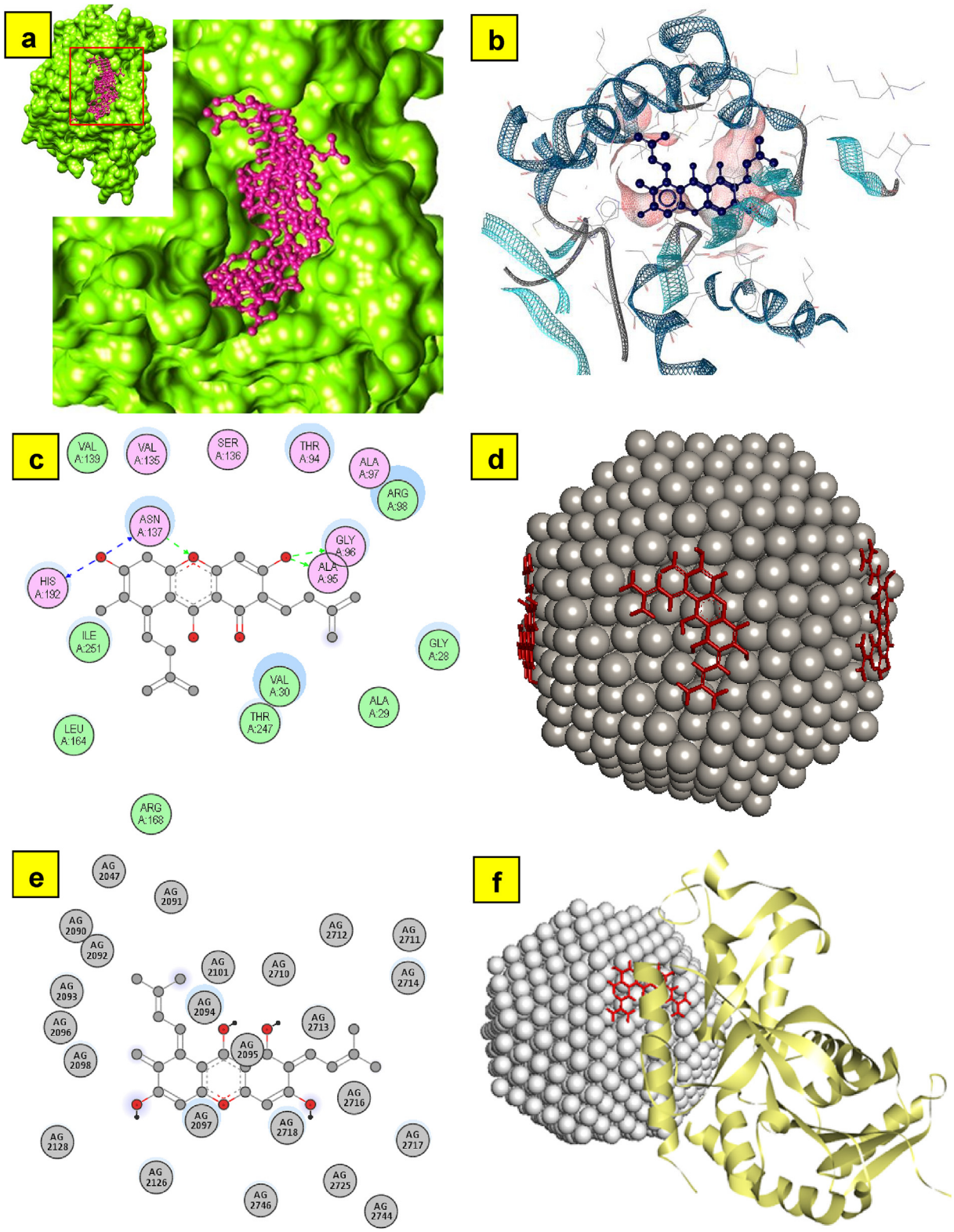

Fig. 6. (a) Docking cluster of α−mangostin within binding pocket of lactate dehydrogenase (LDHA). LDHA protein is shown in green surface representation while ten docked poses of α−mangostin are shown in pink ball and stickDetailed
molecular docking interactions of α−mangostin with LDHA protein; (b) 3D representation of best docked pose of α−mangostin shown in blue ball and stick model while the protein molecule is shown in blue and grey snake model, (c) 2D representation of types of molecular interactions. α−mangostin molecule is shown in grey ball and stick model while the interacting residues are shown in pink (covalent) and green (hydrophobic) discs. Green lines and blue dotted lines represent hydrogen and coordinate covalent bonding, respectively AgNPs-α−mangostin-LDHA interactions; (d) α−mangostin (red ball and stick) conjugated on AgNPs surface (silver), (e) 2D interaction of α−mangostin with AgNPs, (f) interaction of LDHA (yellow ribbon) with α−mangostin conjugated on AgNPs Molecular dynamics simulations trajectories analysis; (g) RMSF plot, (h) superimposed apo and bound stat of LDHA at 10 ns, orange colour represents apo and blue represents α−mangostin bound LDHA protein, and (i) RMSD plot of apo and bound state. (For interpretation of the references to colour in this figure legend, the reader is referred to the Web version of this article.)

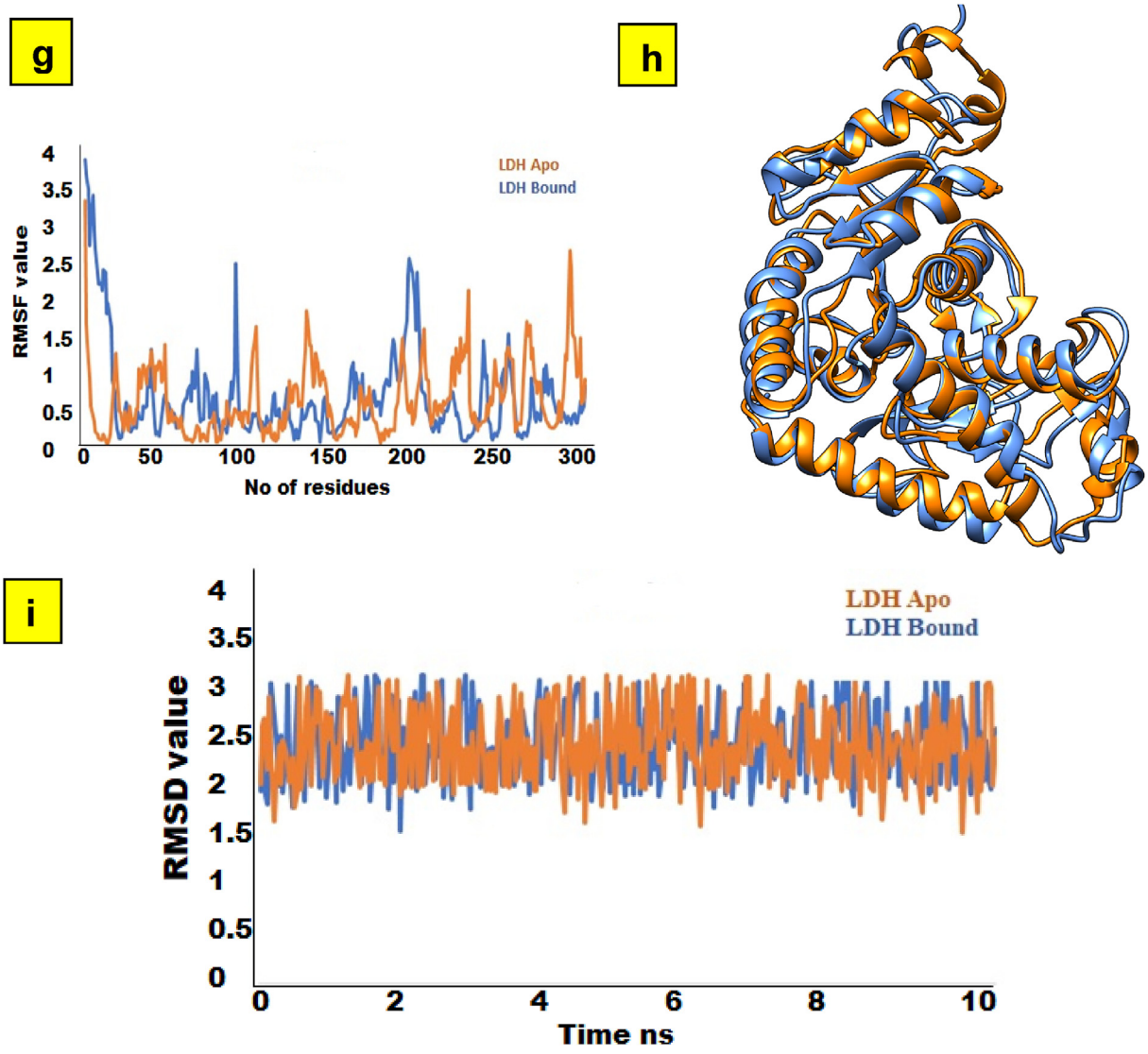

Fig. 6. (*continued*).

fluctuation in and around the binding site residues. The key interacting residues of the LDHA (Gly28, Ala29, Val30, Ala95, Gly96, Arg98, Leu164, His192, Asp197, Ile251, Thr247) showed slight fluctuations to facilitate the binding conformation. Loop and secondary structure elements close to binding site residues showed remarkable fluctuation to aid in the favourable binding pose. Ala95 and Gly96 tilted towards the binding cavity to make H-bond with α-mangostin. His 192 and Asp197 showed inwards movement towards compound to get favourable binding pose. Region encompassing 245 to 251 showed fluctuation to make important interactions. Apart from these regions, far from binding site also showed fluctuation in the loop region (Fig. 6g and h). Overall, RMSD of unbound and bound state of LDHA system showed stability (Fig. 6i).

4. Conclusions

The current study describes the green synthesis of silver nanoparticles by direct interaction of silver nitrate with aqueous, olive, and coconut oil extracts of *G. mangostana* fruit pericarp (unwanted waste material) and its major compound α-mangostin. The GM-AgNPs and Mang-AgNPs were produced prominently in 1:10 ratio under heating and stirring. The presence of phenolic compounds/xanthones in *G. mangostana* fruit pericarp played a key role in the AgNPs synthesis as both reducing and stabilizing agents. The colorimetric sensing of Hg(II) ions demonstrated that GM-AgNPs are cost-effective and efficient towards Hg(II) detection in real water samples. Moreover, GM-AgNPs significantly degraded dyes specifically methylene blue (MB). Hence, the subject AgNPs are promising biosensors and catalysts in Hg(II) detection and dyes reduction. Conclusively, these AgNPs could be beneficial in the fields of environmental remediation and nanomedicine in the future. Furthermore, the subject AgNPs have significant antioxidant, antimicrobial and potential selective action toward prostate cancer line; DU-145 cell line compared to normal human cells. This might be attributed to the presence of hydroxyl (OH) groups in the α-mangostin. Also, the in vitro anticancer potential against DU-145 was validated the best pose scoring by in silico molecular docking studies for the first time.

Author statement

Nargis Jamila: Supervision, Project Administration, Writing-Review & Editing. Naeem Khan: Conceptualization, Resources,

Writing Original Draft, Writing-Review & Editing. Nousheen Bibi: Software, Formal analysis. Muhammad Waqas: Resources, Writing-Review & Editing. Sadiq Noor Khan: Methodology, Resources, Writing Original Draft. Amir Atlas: Invsetigation, Writing Original Draft. Farhat Amin: Resources, Writing-Review & Editing. Faryal Khan: Investigation. Malka Saba: Investigation

Declaration of competing interest

The authors declare that they have no known competing financial interests or personal relationships that could have appeared to influence the work reported in this paper.

Acknowledgement

This research study was supported by the research grant; 8967/KPK/NRPU/R&D/HEC/2017. The authors are thankful to the Higher Education Commission (HEC) for awarding this project.

Appendix A. Supplementary data

Supplementary data to this article can be found online at https://doi.org/10.1016/j.chemosphere.2021.129794.

References

Abbasi, E., Milani, M., Fekri Aval, S., Kouhi, M., Akbarzadeh, A., Tayefi Nasrabadi, H., Niksa, P., Joo, S.W., Hanifehpour, Y., Nijati-Koshki, K., Samiei, M., 2016. Silver nanoparticles: synthesis methods, bio-applications and properties. Crit. Rev. Microbiol. 42, 173–180. https://doi.org/10.3109/1040841X.2014.912200.

Ahmad, F., Ashraf, N., Ashraf, T., Zhou, R.B., Yin, D.C., 2019. Biological synthesis of metallic nanoparticles (MNPs) by plants and microbes: their cellular uptake, biocompatibility, and biomedical applications. Appl. Microbiol. Biotechnol. 103, 2913–2935. https://doi.org/10.1007/s00253-019-09675-5.

Ajaz, M., Shakeel, S., Rehman, A., 2020. Microbial use for azo dye degradation—a strategy for dye bioremediation. Int. Microbiol. 23, 149–159. https://doi.org/10.1007/s10123-019-00103-2.

Alexander, K., Oleksandr, M.K., Iurii, I.G., Sergiy, M.K., Oleg, N.K., 2015. Atomistic simulations of coating of silver nanoparticles with poly(vinylpyrrolidone) oligomers: effect of oligomer chain length. J. Phys. Chem. C 119, 7888–7899. https://doi.org/10.1021/jp510369a.

Bandi, R., Alle, M., Park, C.W., Han, S.Y., Kwon, G.J., Kim, J.C., Lee, S.H., 2020. Rapid synchronous synthesis of Ag nanoparticles and Ag nanoparticles/holocellulose nanofibrils: Hg (II) detection and dye discoloration. Carbohydr. Polym. 240, 116356. https://doi.org/10.1016/j.carbpol.2020.116356.

Bonnia, N.N., Kamaruddin, M.S., Nawawi, M.H., Ratim, S., Azlina, H.N., Ali, E.S., 2016. Green biosynthesis of silver nanoparticles using '*Polygonum hydropiper*' and study its catalytic degradation of methylene blue. Procedia. Chem. 19, 594–602. https://doi.org/10.1016/j.proche.2016.03.058.

Bothra, S., Jignasa, N.S., Suban, K.S., John, F.C., 2014. Anion-driven selective colorimetric detection of Hg^{2+} and Fe^{3+} using functionalized silver nanoparticles. RSC Adv. 4, 1341–1346. https://doi.org/10.1039/C3RA44945A.

Chandraker, S.K., Ghosh, M.K., Lal, M., Ghorai, T.K., Shukla, R., 2019. Colorimetric sensing of Fe^{3+} and Hg^{2+} and photocatalytic activity of green synthesized silver nanoparticles from the leaf extract of *Sonchus arvensis* L. New J. Chem. 43, 18175–18183. https://doi.org/10.1039/C9NJ01338E.

Chen, G., Li, Y., Wang, W., Deng, L., 2018. Bioactivity and pharmacological properties of α-mangostin from the mangosteen fruit: a review. Expert Opin. Ther. Pat. 28, 415–427. https://doi.org/10.1080/13543776.2018.1455829.

Cheok, C.Y., Chin, N.L., Yusof, Y.A., Talib, R.A., Law, C.L., 2013. Optimization of total monomeric anthocyanin (TMA) and total phenolic content (TPC) extractions from mangosteen (*Garcinia mangostana* Linn.) hull using ultrasonic treatments. Ind. Crop. Prod. 50, 1–7. https://doi.org/10.1016/j.indcrop.2013.07.024.

Es'haghi, Z., Vafaeinezhad, F., Hooshmand, S., 2016. Green synthesis of magnetic iron nanoparticles coated by olive oil and verifying its efficiency in extraction of nickel from environmental samples via UV–vis spectrophotometry. Process Saf. Environ. Protect. 102, 403–409. https://doi.org/10.1016/j.psep.2016.04.011.

Gahlawat, G., Choudhury, A.R., 2019. A review on the biosynthesis of metal and metal salt nanoparticles by microbes. RSC Adv. 9, 12944–12967. https://doi.org/10.1039/C8RA10483B.

Guo, Q., Guo, Q., Yuan, J., Zeng, J., 2014. Biosynthesis of gold nanoparticles using a kind of flavonol: Dihydromyricetin. Colloids Surf., A 441, 127–132. https://doi.org/10.1016/j.colsurfa.2013.08.067.

Ismail, M., Khan, M.I., Akhtar, K., Seo, J., Khan, M.A., Asiri, A.M., Khan, S.B., 2019. Phytosynthesis of silver nanoparticles; naked eye cellulose filter paper dual mechanism sensor for mercury ions and ammonia in aqueous solution. J. Mater. Sci. Mater. 30, 7367–7383. https://doi.org/10.1007/s10854-019-01049-x.

Jahangirian, H., Lemraski, E.G., Webster, T.J., Rafiee-Moghaddam, R., Abdollahi, Y., 2017. A review of drug delivery systems based on nanotechnology and green chemistry: green nanomedicine. Int. J. Nanomed. 12, 2957, 10.2147%2FIJN.S127683.

Jamila, N., Khairuddean, M., Yaacob, N.S., Kamal, N.N.S.N.M., Osman, H., Khan, S.N., Khan, N., 2014. Cytotoxic benzophenone and triterpene from *Garcinia hombroniana*. Bioorg. Chem. 54, 60–67. https://doi.org/10.1016/j.bioorg.2014.04.003.

Jamila, N., Khan, N., Khan, I., Khan, A. A., Khan, S. N., 2016. A bioactive cycloartane triterpene from *Garcinia hombroniana*. Nat. Prod. Res. 30, 1388-1397.https://doi.org/10.1080/14786419.2015.1060594.

Khan, S.A., Khan, S.B., Farooq, A., Asiri, A.M., 2019. A facile synthesis of CuAg nanoparticles on highly porous ZnO/carbon black-cellulose acetate sheets for nitroarene and azo dyes reduction/degradation. Int. J. Biol. Macromol. 130, 288–299. https://doi.org/10.1016/j.ijbiomac.2019.02.114.

Kumar, B., Smita, K., Cumbal, L., Debut, A., 2017. Green synthesis of silver nanoparticles using Andean blackberry fruit extract. Saudi J. Biol. Sci. 24, 45–50. https://doi.org/10.1016/j.sjbs.2015.09.006.

Lee, X.K., Shameli, K., Miyake, M., Kuwano, N., Bt Ahmad Khairudin, N.B., Bt Mohamad, S.E., Yew, Y.P., 2016. Green synthesis of gold nanoparticles using aqueous extract of *Garcinia mangostana* fruit peels. J. Nanomater. 2016. https://doi.org/10.1155/2016/8489094.

Lee, K.X., Shameli, K., Mohamad, S.E., Yew, Y.P., Mohamed Isa, E.D., Yap, H.Y., Lim, W.L., Teow, S.Y., 2019. Bio-Mediated synthesis and characterisation of silver nanocarrier, and its potent anticancer action. Nanomaterials 9, 1423. https://doi.org/10.3390/nano9101423.

Linic, S., Aslam, U., Boerigter, C., Morabito, M., 2015. Photochemical transformations on plasmonic metal nanoparticles. Nat. Mater. 14, 567–576. https://doi.org/10.1038/nmat4281.

Lucky, S.S., Soo, K.C., Zhang, Y., 2015. Nanoparticles in photodynamic therapy. Chem. Rev. 115, 1990–2042. https://doi.org/10.1021/cr5004198.

Morris, G.M., Huey, R., Lindstrom, W., Sanner, M.F., Belew, R.K., Goodsell, D.S., Olson, A.J., 2009. Autodock4 and AutoDockTools4: automated docking with selective receptor flexiblity. J. Comput. Chem. 16, 2785–2791. https://doi.org/10.1002/jcc.21256.

Pandey, S., Do, J.Y., Kim, J., Kang, M., 2020. Fast and highly efficient catalytic degradation of dyes using κ-carrageenan stabilized silver nanoparticles nanocatalyst. Carbohydr. Polym. 230, 115597. https://doi.org/10.1016/j.carbpol.2019.115597.

Park, J.S., Ahn, E.Y., Park, Y., 2017. Asymmetric dumbbell-shaped silver nanoparticles and spherical gold nanoparticles green-synthesized by mangosteen (*Garcinia mangostana*) pericarp waste extracts. Int. J. Nanomed. 12, 6895. https://doi.org/10.2147/IJN.S140190.

Pelgrift, R.Y., Friedman, A.J., 2013. Nanotechnology as a therapeutic tool to combat microbial resistance. Adv. Drug Deliv. Rev. 65, 1803–1815. https://doi.org/10.1016/j.addr.2013.07.011.

Pettersen, E.F., Goddard, T.D., Huang, C.C., Couch, G.S., Greenblatt, D.M., Meng, E.C., Ferrin, T.E., 2004. UCSF Chimera–a visualization system for exploratory research and analysis. J. Comput. Chem. 13, 1605–1612. https://doi.org/10.1002/jcc.20084.

Priya, K., Vijayakumar, M., Janani, B., 2020. Chitosan-mediated synthesis of biogenic silver nanoparticles (AgNPs), nanoparticle characterisation and in vitro assessment of anticancer activity in human hepatocellular carcinoma HepG2 cells. Int. J. Biol. Macromol. 149, 844–852. https://doi.org/10.1016/j.ijbiomac.2020.02.007.

Priyadarshini, E., Pradhan, N., 2017. Gold nanoparticles as efficient sensors in colorimetric detection of toxic metal ions: a review. Sensor. Actuator. B Chem. 238, 888–902. https://doi.org/10.1016/j.snb.2016.06.081.

Raghavan, B.S., Kondath, S., Anantanarayanan, R., Rajaram, R., 2015. Kaempferol mediated synthesis of gold nanoparticles and their cytotoxic effects on MCF-7 cancer cell line. Process Biochem. 50, 1966–1976. https://doi.org/10.1016/j.procbio.2015.08.003.

Rajakannu, S., Shankar, S., Perumal, S., Subramanian, S., Dhakshinamoorthy, G.P., 2015. Biosynthesis of silver nanoparticles using *Garcinia mangostana* fruit extract and their antibacterial, antioxidant activity. Int. J. Curr. Microbiol. Appl. Sci. 4, 944–952.

Ramos-Sanchez, J.E., Camposeco, R., Lee, S.W., Rodríguez-González, V., 2020. Sustainable synthesis of AgNPs/strontium-titanate-perovskite-like catalysts for the photocatalytic production of hydrogen. Catal. Today 341, 112–119. https://doi.org/10.1016/j.cattod.2019.08.020.

Rani, P., Kumar, V., Singh, P.P., Matharu, A.S., Zhang, W., Kim, K.-H., Singh, J., Rawat, M., 2020. Highly stable AgNPs prepared via a novel green approach for catalytic and photocatalytic removal of biological and non-biological pollutants. Environ. Int. 143, 105924. https://doi.org/10.1016/j.envint.2020.105924.

Samprasit, W., Akkaramongkolporn, P., Jaewjira, S., Opanasopit, P., 2018. Design of alpha mangostin-loaded chitosan/alginate controlled-release nanoparticles using genipin as crosslinker. J. Drug Deliv. Sci. Technol. 46, 312–321. https://doi.org/10.1016/j.jddst.2018.05.029.

Sana, S.S., Dogiparthi, L.K., 2018. Green synthesis of silver nanoparticles using *Givotia moluccana* leaf extract and evaluation of their antimicrobial activity. Mater. Lett. 226, 47–51. https://doi.org/10.1016/j.matlet.2018.05.009.

Sarwar, N., Imran, M., Shaheen, M.R., Ishaque, W., Kamran, M.A., Matloob, A., Abdur, R., Hussain, S., 2017. Phytoremediation strategies for soils contaminated with heavy metals: modifications and future perspectives. Chemosphere 171, 710–721. https://doi.org/10.1016/j.chemosphere.2016.12.116.

Sengan, M., Veeramuthu, D., Veerappan, A., 2018. Photosynthesis of silver nanoparticles using *Durio zibethinus* aqueous extract and its application in catalytic reduction of nitroaromatics, degradation of hazardous dyes and selective colorimetric sensing of mercury ions. Mater. Res. Bull. 100, 386–393. https://doi.org/10.1016/j.materresbull.2017.12.038.

Tousian, H.S., Razavi, B.M., Hosseinzadeh, H., 2017. Review of *Garcinia mangostana* and its xanthones in metabolic syndrome and related complications. Phytother Res. 31, 1173–1182. https://doi.org/10.1002/ptr.5862.

Veerasamy, R., Xin, T.Z., Gunasagaran, S., Xiang, T.F.W., Yang, E.F.C., Jeyakumar, N., Dhanaraj, S.A., 2011. Biosynthesis of silver nanoparticles using mangosteen leaf extract and evaluation of their antimicrobial activities. J. Saudi Chem. Soc. 15, 113–120. https://doi.org/10.1016/j.jscs.2010.06.004.

Venugopal, K., Rather, H.A., Rajagopal, K., Shanthi, M.P., Sheriff, K., Illiyas, M., Rather, R.A., Manikandan, E., Uvarajan, S., Haskar, M., Maaza, M., 2017. Synthesis of silver nanoparticles (Ag NPs) for anticancer activities (MCF 7 breast and A549 lung cell lines) of the crude extract of *Syzygium aromaticum*. J. Photochem. Photobiol., B 167, 282–289. https://doi.org/10.1016/j.jphotobiol.2016.12.013.

Vo, T.T., Dang, C.H., Doan, V.D., Dang, V.S., Nguyen, T.D., 2020. Biogenic synthesis of silver and gold nanoparticles from *Lactuca indica* leaf extract and their application in catalytic degradation of toxic compounds. J. Inorg. Organomet. Polym. Mater. 30, 388–399. https://doi.org/10.1007/s10904-019-01197-x.

Wang, Y., Yang, F., Yang, X., 2010. Colorimetric detection of mercury (II) ion using unmodified silver nanoparticles and mercury-specific oligonucleotides. ACS Appl. Mater. Interfaces 2, 339–342. https://doi.org/10.1021/am9007243.

Yoo, J.W., Irvine, D.J., Discher, D.E., Mitragotri, S., 2011. Bio-inspired, bioengineered and biomimetic drug delivery carriers. Nat. Rev. Drug Discov. 10, 521–535. https://doi.org/10.1038/nrd3499.

Zarena, A.S., Sankar, K.U., 2012. Phenolic acids, flavonoid profile and antioxidant activity in mangosteen (*Garcinia Mangostana* L.) pericarp. J. Food Biochem. 36, 627–633. https://doi.org/10.1111/j.1745-4514.2011.00575.x.